Applied Catalysis B: Environmental 90 (2009) 262–267

Contents lists available at ScienceDirect

Applied Catalysis B: Environmental

journal homepage: www.elsevier.com/locate/apcatb

Fabrication of crack-free anodic nanoporous titania and its enhanced photoelectrochemical response

Guoge Zhang [a], Haitao Huang [a,*], Yuanshuai Liu [b], Limin Zhou [c]

[a] Department of Applied Physics and Materials Research Center, the Hong Kong Polytechnic University, Hung Hom, Kowloon, Hong Kong
[b] Department of Applied Biology and Chemical Technology, the Hong Kong Polytechnic University, Hung Hom, Kowloon, Hong Kong
[c] Department of Mechanical Engineering, the Hong Kong Polytechnic University, Hung Hom, Kowloon, Hong Kong

ARTICLE INFO

Article history:
Received 11 December 2008
Received in revised form 20 February 2009
Accepted 5 March 2009
Available online 19 March 2009

Keywords:
Titania nanotube
Photocatalyst
Electrochemical anodization
Antibacterial test
Photo-decomposition

ABSTRACT

Crack-free nanoporous titania was fabricated with an appropriate post-anodization treatment. Such a nanoporous structure shows enhanced photoelectrochemical response as compared to the conventional nanotubular titania of similar thickness. The enhanced photocatalytic activity is demonstrated through the photo-degradation of methyl orange and antibacterial-drop test, and is thought to result from the more efficient electron–hole separation in the porous structure. Further improvement in the photocatalytic efficiency can be achieved on thicker titania layers fabricated by extended anodization. This kind of nanostructured titania may find its potential applications in bactericidal process, photocatalytic decomposition of organic contamination, and wastewater purification.

1. Introduction

Photocatalytic degradation of organic compound is of great importance to the elimination of hazardous wastes [1]. Semiconducting TiO_2 as a durable photocatalyst has been widely studied for water and air purification [2]. For applications in pollution control, most research work was focused on nanoparticulate films or suspensions [3–6]. The photocatalytic activity of nanoparticulate film is limited by the small surface area, while for the particulate suspension, removal of the catalyst after use is technologically expensive and difficult. TiO_2 nanotube array made by electrochemical anodization was claimed to possess higher catalytic efficiency than the nanoparticulate film does [7,8]. However, there is an intrinsic limit on the photoelectrochemical response of the TiO_2 nanotube array due to its small wall thickness [9].

There have been extensive reports on the synthesis of anodic titania in aqueous or organic electrolytes [10–16] containing fluoride, chloride, or bromide [17–21]. In chloride or bromide solution, due to restricted electrochemical conditions, the anodized titania shows a much faster growth rate with less ordered morphology and less tunable dimensions than it does in fluoride solution. For anodization in aqueous electrolyte with fluoride, the length of nanotubes is determined by two competing factors, i.e., the formation of titania at TiO_2–Ti interface and the dissolution of titania at tube mouth. Due to the high dissolution speed of TiO_2 in acidic environment, the length of nanotubes is normally in the range of several hundred nanometers to a few micrometers. When organic electrolyte is used, the chemical dissolution of TiO_2 is negligible and much longer TiO_2 nanotubes could be obtained simply by the extension of anodization time [10]. However, the top surface of thus obtained TiO_2 was covered by a layer of TiO_2 nanowires, which might reduce the adsorption of organic dye and thus limit the applications in dye-sensitized solar cells or in waste water purification. The attempt to remove such surface debris by ultrasonic cleaning in deionized water is not successful as ultrasonication also results in shattered anodic TiO_2 layer [10]. By adopting a "self templating" method, highly order nanoporous anodic TiO_2 has been synthesized without the unwanted nanowire layer and has showed better photodegradation activity than nanotubular TiO_2 [22]. However, the detailed mechanism of such enhanced photoelectrochemical response was still not very clear. Another unsolved problem for this nanoporous anodic TiO_2 was that surface cracks can be easily produced when the sample is washed with deionized water directly after anodization, as shown in Fig. 1(a). In some occasions the nanostructured TiO_2 even peeled off, as shown in Fig. 1(b). Since a crack-free surface of anodic TiO_2 is crucial for many potential applications, in the present work, we will focus on the fabrication of crack-free anodic nanoporous TiO_2 films.

It has been reported that a small amount of F^- was always found in the as-anodized TiO_2 [23]. When it was washed with deionized

* Corresponding author. Tel.: +852 2766 5694; fax: +852 2333 7629.
E-mail address: aphhuang@polyu.edu.hk (H. Huang).

0926-3373/$ – see front matter © 2009 Elsevier B.V. All rights reserved.
doi:10.1016/j.apcatb.2009.03.012

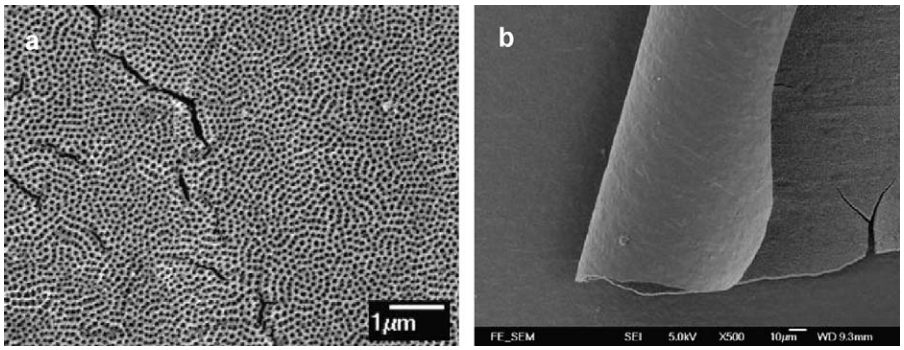

Fig. 1. FSEM images showing (a) cracks in nanoporous structure and (b) peeling off of TiO_2 film for anodic samples without appropriate post-anodization treatment.

water right after anodization, the residual F^- ions might hydrolyze to generate HF and lead to the dissolution of TiO_2. Such etching process would result in surface cracks and even peeling off of the film. The dissolution of TiO_2 in F^- containing electrolyte is highly dependent on the pH value of the solution, with acidic environment as the requisite [13]. There is no chemical etching for TiO_2 in F^- containing non-aqueous solution. Therefore, a very straightforward method to produce crack-free anodic TiO_2 is the post-anodization treatment in certain organic solvent which has high solubility of F^- ions to remove the residual F^- ions. In this paper, we will describe how crack-free nanoporous TiO_2 is obtained through a simple process. The photoelectrochemical response of the obtained nanoporous TiO_2 will be examined and compared with the conventional tubular TiO_2. An improved photocatalytic activity in nanoporous TiO_2 is demonstrated through the decomposition of methyl orange (MO) and antibacterial study. The detailed mechanism behind this enhancement is investigated. This kind of nanostructured TiO_2 may find its important applications not only in bactericidal process, wastewater purification and photocatalytic decomposition of organic contamination, but also in photocleavage of water and dye-sensitized solar cells.

2. Experimental

The detailed methodology of fabricating highly ordered anodic nanoporous titania has been published elsewhere [22]. Hence only the key points of the anodization process are summarized here. Titanium foils (0.25 mm thickness, 99.6% purity, Strem Chemicals, USA) were degreased ultrasonically in acetone and ethanol for 10 min, respectively, followed by rinsing with deionized water and drying in hot air. The anodization voltage was set at 50 V and the electrolyte was ethylene glycol with the addition of 0.25 wt.% NH_4F. No water was added in order to suppress the chemical dissolution of TiO_2 in the electrolyte. The lack of chemical dissolution is crucial in obtaining the porous structure. In our previous work, a three-step anodization was carried out to achieve the perfectly ordered structure [22]. In this study, the aim is to produce crack-free films. To save time, a two-step anodization process was adopted to produce nanoporous TiO_2. For the first step, the potential was ramped at a rate of 0.5 V/s to 50 V. For the second step, a voltage of 50 V was applied instantaneously at the beginning of anodization. The anodization time was 4 h in the first step. The as-anodized sample was then ultrasonically cleaned in deionized water for 5 min to remove the anodic TiO_2 layer from the titanium substrate. Afterwards, the exposed titanium substrate was subjected to the second anodization for different duration (5 and 100 min, respectively) to create nanoporous TiO_2 layer with different thickness. To achieve crack-free nanoporous structure, the as-grown TiO_2 layer was placed into a methanol bath with the anodized surface facing upward. After 3 days' soaking, the sample was taken out and washed thoroughly with deionized water. For the comparison of the photocatalytic activity, nanotubular TiO_2 was electrochemically anodized in 0.2 wt.% HF aqueous solution. The anodization time and voltage were 30 min and 20 V, respectively.

The morphology of the anodic TiO_2 was examined by field emission scanning electron microscope (FESEM, JEOL JSM-6335F). Both tubular and porous as-anodized TiO_2 were amorphous. They were crystallized to anatase phase after being annealed at 450 °C for 3 h, with a heating rate of 4 °C/min. X-ray diffraction (XRD, Philips PW3020) analysis was carried out to investigate the crystal structure. The electrochemical measurements were performed in a standard three-electrode configuration, with platinum the counter electrode and saturated calomel electrode (SCE) the reference. The photocurrent was measured using an electrochemical workstation (CHI 660B) with a UV lamp (central wavelength: 369 nm, irradiation intensity: 6 W/m^2) as the light resource and 0.1 M H_2SO_4 as the electrolyte. The sweep rate of the potential was 0.05 V/s. The photo-decomposition of MO solution (12 mg L^{-1}) was carried out under the illumination of the same UV lamp as used in the photocurrent measurement. The nanostructured TiO_2 was under normal incidence with a distance of 4 cm to the UV source. Titanium foil without anodization was used as a blank. The change of MO concentration with the radiation time was monitored by measuring the absorbance of MO solution at a wavelength of 464 nm using a UV–vis spectrophotometer (Shimadzu, UV-2550). The bactericidal activity against *Staphylococcus aureus* (SA) was studied using the antibacterial-drop test [24]. SA was cultivated in Luria-Bertani (LB) medium at 37 °C for 24 h and diluted to the concentration around 10^7 colony forming units per milliliter (CFU ml^{-1}). Then 100 μl bacteria containing solution was added dropwise onto the surface of anodic TiO_2 with an area of 6 cm^2. The test was carried out at room temperature for 0.5, 1 and 2 h. After each time period the bacteria containing drops were washed away from the samples using 20 ml double distilled water. Then 40 μl of each bacteria suspension was dispersed on the agar plate. The number of surviving bacteria was counted after incubation for 24 h at 37 °C.

3. Results and discussion

3.1. Morphology and microstructure characterization

Fig. 2 shows the SEM images of anodic TiO_2 after the post-anodization treatment (3 days' soaking in methanol and thorough washing with deionized water). The diameter of pores is around 60 nm and the interpore distance ranges from 130 to 150 nm. Nanoporous structure can be clearly seen and is different from the conventional tubular morphology [10–15,17]. Such regular nanostructure is very similar to that of the anodic aluminium or titanium aluminide [25–27], and is the result of preferred pore nucleation in self-templated titanium substrate [22]. The cross-section image

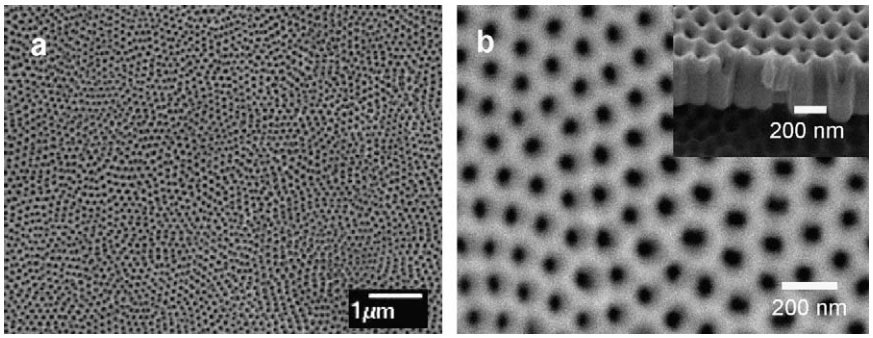

Fig. 2. SEM images of crack-free nanoporous TiO_2: (a) low and (b) high magnifications. The inset in (b) shows the cross-section of the anodic layer.

shows that the fracture takes place along the boundaries of TiO_2 cells, indicating that the junction sites are mechanically weaker than TiO_2 cell walls. Compared with Fig. 1, the synthesized TiO_2 layer is totally crack-free. The adhesion strength between TiO_2 and titanium substrate is also increased after soaking in methanol. No peeling off of the TiO_2 layer happened after 5 min wash in ultrasonic bath in deionized water, which is in sharp contrast to the easily peeled off as-anodized titania layer without any treatment in methanol. Such improvement in mechanical property is promising in terms of applications for anodic TiO_2, where the sample stability is crucial for long term use.

Energy dispersive X-ray (EDX) spectrum was conducted to analyze the elemental content in anodic TiO_2 with (and without) soaking in methanol bath. Fig. 3(a) shows the result of as-grown TiO_2 (without treatment in methanol) after thorough washing in deionized water. Fluorine peak can be identified where the amount of F^- is estimated to be about 7 at.%. This anion uptake is quite common for oxide layers grown electrochemically in either aqueous or organic electrolyte [23,28]. F^- may hydrolyze with water to form HF, leading to the slow chemical dissolution of TiO_2, and result in surface cracks as shown in Fig. 1(a). Due to the low surface tension ($\gamma_{CH_3OH} = 22.1$ dynes/cm at 20 °C) [29], methanol can easily penetrate into TiO_2 cell and reach the bottom of the pores. At the same time, methanol is fully miscible with ethylene glycol and has a high solubility of NH_4F. These two factors make it easy for the fluorine species to leave TiO_2 cells and to be dissolved in methanol. Fig. 3(b) presents the EDX analysis of anodic TiO_2 after 3 days' soaking in methanol. As expected, no fluorine can be detected. The chemical dissolution of TiO_2 is thus negligible in subsequent washing with deionized water. As a result, the surface of methanol-treated nanoporous TiO_2 is intact and totally crack-free. There is also no attack on the barrier layer between the anodic TiO_2 and titanium substrate, and thus no loss of the adhesion strength.

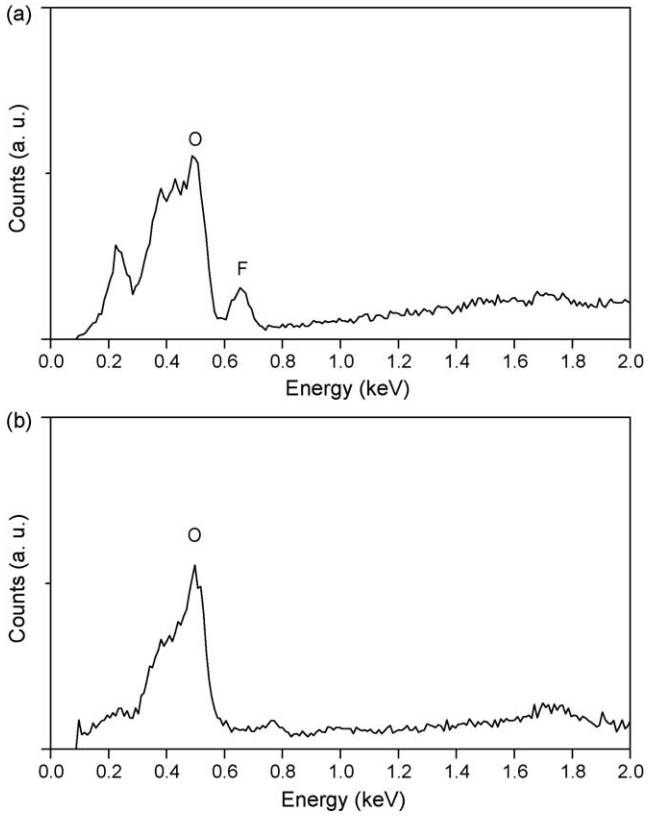

Fig. 3. EDX of as-grown anodic TiO_2 (a) before and (b) after treatment in methanol bath.

To evaluate the photocatalytic properties of nanoporous TiO_2, nanotubular anodic TiO_2 was fabricated for comparison. Fig. 4(a) shows the nanotubular TiO_2 anodized in HF aqueous solution. The electrolyte concentration, anodization voltage and time were fine tuned so that the nanotube layer is of the same thickness (300–400 nm) and interpore distance (130–150 nm) as that of the nanoporous TiO_2.

The photocatalytic performance of anodic TiO_2 is determined by many factors, such as, surface area, pH value of the solution, diffusion rate, crystalline structure and film thickness. Among these factors, crystalline structure is believed to be the most critical one. Amorphous titania shows negligible photocatalytic activity while anatase is constantly more active than rutile [30,31]. For a meaningful comparison on the photocatalytic properties of nanoporous and nanotubular TiO_2, heat treatment should be conducted to ensure that both types of materials are of the same phase. Fig. 4(b) shows the XRD patterns of as-anodized TiO_2 annealed at 450 °C for 3 h. Both nanoporous and nanotubular TiO_2 are in anatase phase with (1 0 1) peak at 25.4° and (2 0 0) peak at 48.2°. No rutile phase can be detected. There were also no discernible changes in surface morphology (SEM images not shown here) for both materials after the annealing.

3.2. Photocatalytic degradation of methyl orange

The photocatalytic property of annealed anodic TiO_2 was evaluated by the photo-decomposition of an organic color indicator, MO, under UV illumination. The kinetics of the decomposition reaction was evaluated by the following equation [32],

$$\ln\left(\frac{C_0}{C}\right) = \ln\left(\frac{A_0}{A}\right) = kt \quad (1)$$

where C_0 and C are the concentrations of methyl orange before and after UV irradiation, A_0 is the absorbance of MO solution at

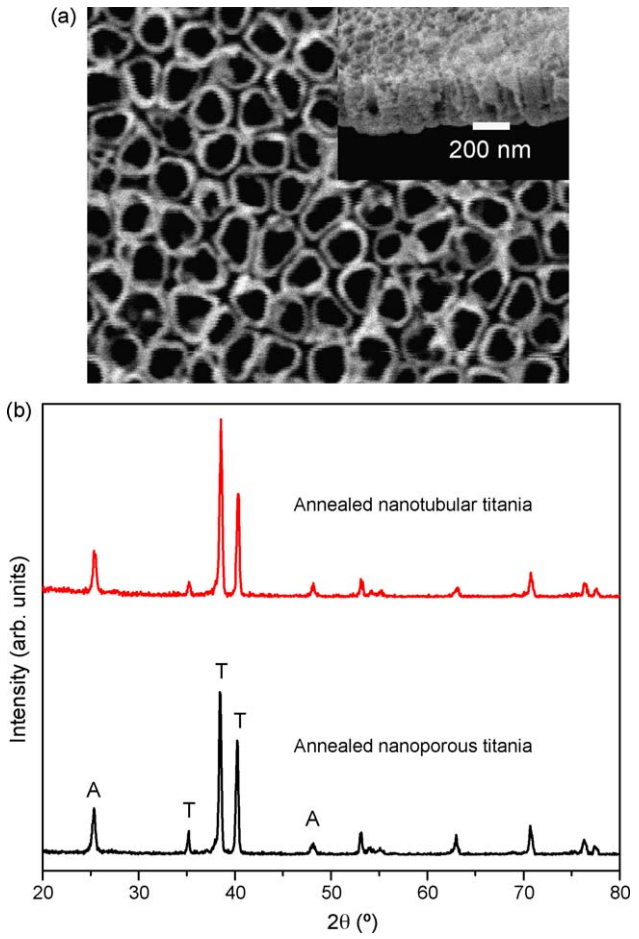

Fig. 4. (a) SEM images of nanotubular TiO_2, inset shows the cross-section. (b) XRD patterns of annealed anodic TiO_2. T: titanium, A: anatase.

a wavelength of 464 nm measured before UV irradiation, A is the absorbance after the UV irradiation for a period of time t, and k is the rate constant. Fig. 5 shows the kinetic behaviors of the decomposition of MO by the anodic nanostructured TiO_2. Without TiO_2 photocatalyst (blank test), the decomposition of MO is negligible under UV illumination. The decoloration of MO solution became significant when annealed TiO_2 was used. It can be clearly seen that the color of dye disappeared at a faster rate for

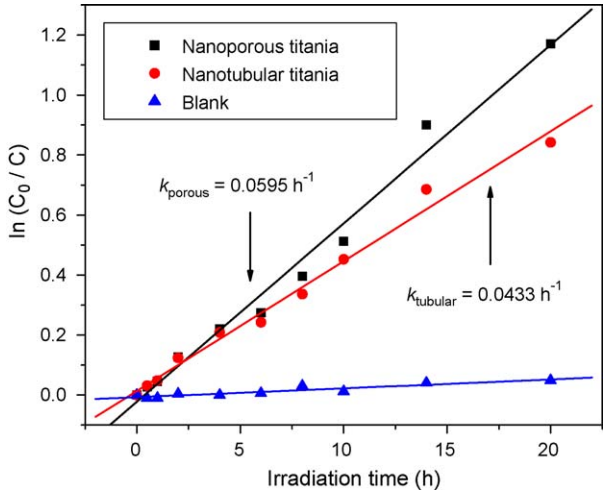

Fig. 5. Decomposition of MO by nanoporous and nanotubular TiO_2.

nanoporous TiO_2 than that for nanotubular TiO_2, where the rate constants are 0.0595 and 0.0433 h^{-1}, respectively. The degradation efficiency of nanoporous TiO_2 is consistently higher over the entire test period. It should be noted that the rate constant of anodic TiO_2 in this study was lower than what was reported elsewhere [8]. Such difference was caused by the difference in experimental conditions, especially in that a much weaker UV irradiation intensity (6 W m^{-2} vs. 600 W m^{-2} in Ref. [8]) was used in the present investigation.

3.3. Photoelectrochemical response

Besides the crystalline phase, the amount of organic dye absorbed on the surface of TiO_2 photocatalyst is also considered as a critical factor determining photo-degradation efficiency [33]. Surface area of nanotubular TiO_2 is considered to be larger than that of nanoporous one due to its larger pore diameter and the dissolved interpore area. As both materials show almost the same XRD patterns and similar solution wettability (contact angle is 4.3 and 3.7° for nanoporous and nanotubular TiO_2, respectively), the absorbed amount of MO is expected to be higher on the surface of nanotubular TiO_2. In this respect, a better photocatalytic activity should be observed for nanotubular TiO_2. However, the experimental result (Fig. 5) shows the opposite. Such a contradictory result could be due to the fact that the dye adsorption amount on the surface of both materials is high enough so that it is no longer the rate limiting factor in the photocatalytic reaction.

The electron–hole recombination kinetics is considered as one of the most important factors that control the photocatalytic activity [34–36]. Slow charge recombination normally leads to high photocatalytic efficiency. The separation of an electron–hole pair is assisted by the action of electric field in depletion region [37]. The greater the band bending potential, the less is the chance for charge recombination. A complete depletion layer cannot be formed in very small nanoparticles that are only a few nanometers in size [38]. Generally speaking, in nanostructured materials, the band bending potential is reduced as the particle size is decreased. As demonstrated by Beranek et al. [9], there is a natural limit of the photoelectrochemical response in anodic TiO_2 nanotubes due to thin tube walls. The wall thickness of nanoporous TiO_2 is around 80 nm, much thicker than that of the nanotubular one (15 nm). It can thus be anticipated that nanoporous TiO_2 has greater band bending potential which results in more efficient charge separation. From the transient study shown below, we can see that it is the slow charge recombination that leads to the enhanced photocatalytic activity in nanoporous TiO_2.

The recombination kinetics of the photogenerated electron–hole pairs was studied through the decay measurement of the open circuit potential (OCP) using the technique described by Zaban et al. [39]. The variation of OCP when the UV lamp is switched on and off is shown in Fig. 6(a). For both types of nanostructured TiO_2, photo-induced delocalized electrons are accumulated in the conduction band of TiO_2 under UV illumination and they then migrated to Ti substrate, leading to a negative shift of OCP. The change of OCP is larger for nanoporous TiO_2, indicating more electrons generated. When UV illumination is switched off, free electrons recombine with the holes, resulting in the decay of potential. The potential decay rate is related to the electron lifetime by the following equation,

$$\tau = \frac{kT}{q}\left(\frac{dV_{oc}}{dt}\right)^{-1} \quad (2)$$

where k is the Boltzmann constant, T is the absolute temperature, q is the positive elementary charge, and dV_{oc}/dt is the derivative of the transient OCP. The calculated electron lifetime does not in

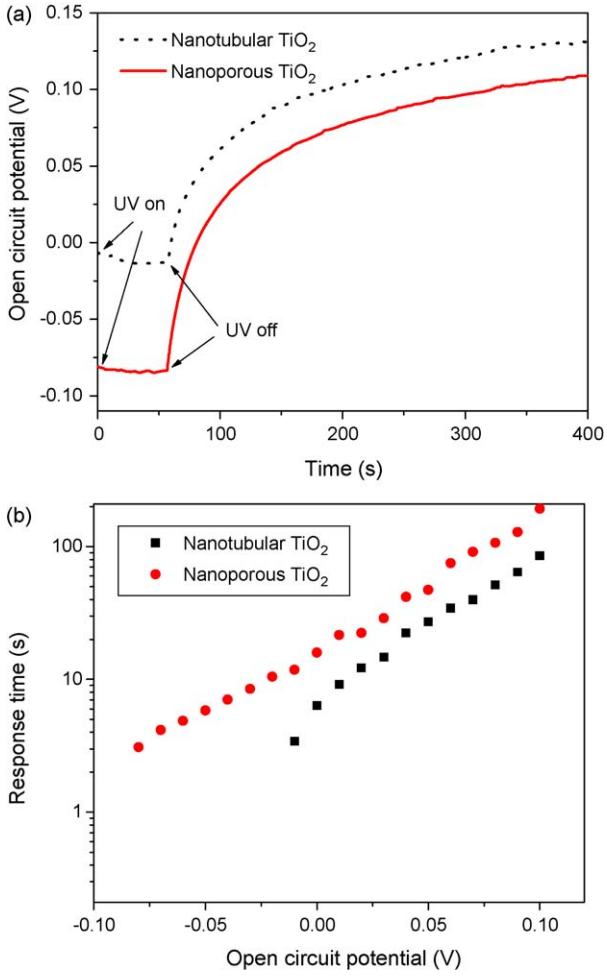

Fig. 6. (a) OCP decay measurement on nanoporous and nanotubular TiO_2. (b) Response time determined by OCP decay on nanoporous and nanotubular TiO_2.

general correspond to the free carrier lifetime but is an average of the characteristic time for the survival of free and trapped electrons [39]. As shown in Fig. 6(b), for both materials the lifetime increases approximately exponentially with increasing potential. Nanoporous TiO_2 exhibits longer lifetime than nanotubular one does, indicating a more efficient separation of the photo-generated electron–hole pairs. Consequently, the organic dye absorbed on TiO_2 surface has more opportunity to be oxidized by holes or by hydroxyl radicals ($^{\bullet}OH$) and superoxide ions ($^{\bullet}O_2^-$), which are produced through the reaction of photo-generated charges with surface absorbed H_2O or O_2 molecules [40]. As a result, faster dye degradation rate was observed.

Fig. 7 shows the variation of photocurrent density with potential for two types of anodic nanostructured TiO_2. Both curves exhibit the typical shape of an *n*-type semiconductor. The dark current densities of these two materials are negligibly small. Under UV illumination, the photocurrent density is increased significantly. The curve slope is steeper for nanoporous TiO_2 and enhanced photocurrent is observed essentially over the entire potential range. At a potential of 1.2 V, the photocurrent density of nanoporous TiO_2 is about twice the value of nanotubular one. As discussed in Fig. 6(a), the shift of OCP is more negative for nanoporous TiO_2 which is believed to be the result of more accumulated photo-generated electrons. This readily explains the higher photocurrent at low potentials observed in Fig. 7. As potential is increased, the band bending in nanostructured film is also increased, leading to decreased charge recombination rate and

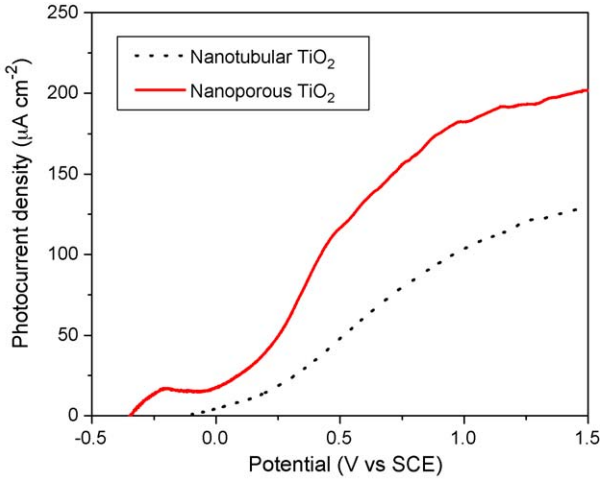

Fig. 7. Variation of the photocurrent density with potential (vs. SCE) in nanoporous and nanotubular TiO_2.

thus enhanced photocurrent. The enhanced photocurrent is more notable before the space charge layer occupies the entire material [9].

The photoconversion efficiency E_{eff} of light to chemical energy in the presence of an external applied potential can be expressed as [41],

$$E_{eff} = j_p \frac{E^0_{rev} - |E_{app}|}{I_0} \times 100 \quad (3)$$

where j_p is the photocurrent density, E^0_{rev} is the standard reversible potential (1.23 V), I_0 is the irradiation intensity of the incident light, and E_{app} is the applied potential, which is difference between the electrode potential (at which j_p was measured) and OCP in the same electrolyte and under the same illumination. Fig. 8 shows the photoconversion efficiency of nanotubular and nanoporous TiO_2. The higher photoconversion efficiency for nanoporous TiO_2 exhibits the advantage of this nanostructure. A maximum conversion efficiency of 10.85% is obtained at 0.48 V vs. SCE.

3.4. Antibacterial investigation

Although there are several photo-degradation studies of anodic TiO_2 [7,8], the antibacterial investigation is still very limited. Both

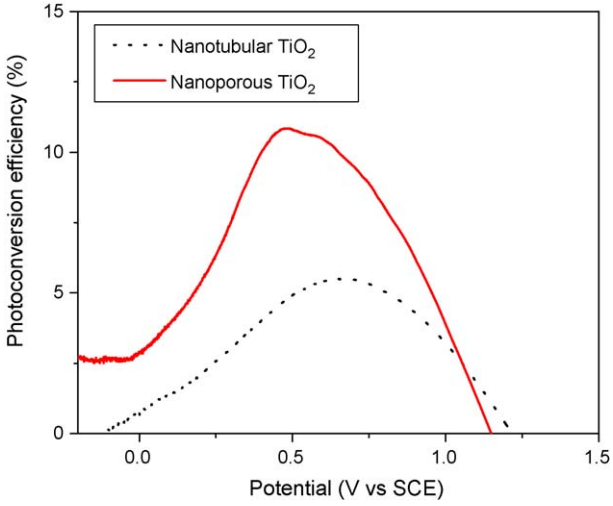

Fig. 8. Photoconversion efficiency as a function of potential (vs. SCE) for nanoporous and nanotubular TiO_2.

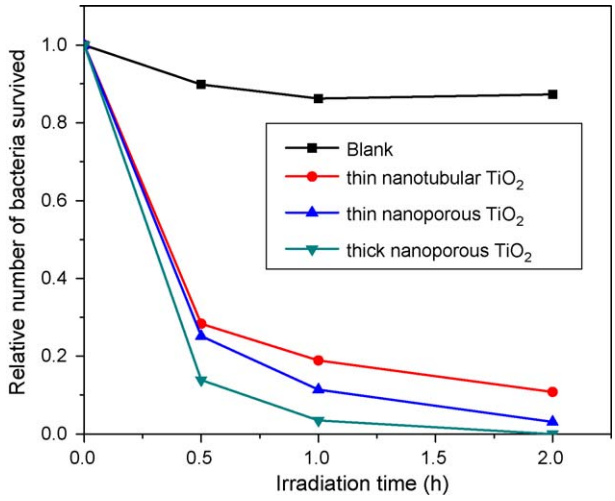

Fig. 9. Relative number of bacteria survived on the surface of different substrates under UV illumination.

TiO_2 particles and films were reported to be promising in bactericidal process [42,43]. As anodic TiO_2 layer is more efficient than TiO_2 particulate film in the photo-degradation of organic dyes [7,8], it would be of great interest to test the antibacterial activity of anodic TiO_2. The result of the bactericidal test is shown in Fig. 9, where the relative number of bacteria survived is the ratio between survived number and the initial number. To investigate the effect of TiO_2 layer thickness, thicker nanoporous TiO_2 (7 μm) which was obtained after extended second step anodization (100 min), was also tested.

There was a marginal decrease in the survived bacteria number for the blank test under UV illumination. Due to the strong oxidization power of anodic TiO_2 under UV illumination, all the three nanostructured TiO_2 layers showed good bactericidal activities. The thicker nanoporous anodic TiO_2 exhibited the best antibacterial performance. No viable cells were found after UV irradiation for 2 h. The CFU reduction from over 1000 to 0 is remarkable and the bactericidal effect is very impressive. For thinner anodic layers (around 350 nm), nanoporous TiO_2 is more efficient than tubular one for all the test period. Such enhancement is also caused by the slower recombination of electron–hole pairs. The CFUs after UV irradiation for 2 h were 31 and 106 for nanoporous and nanotubular TiO_2, respectively. This result coincides with the photo-degradation result.

4. Conclusion

In summary, crack-free anodic nanoporous TiO_2 is fabricated with an appropriate post-anodization treatment. Such material shows improved adhesion strength to the Ti substrate which is attractive for long term applications. Compared to the nanotubular TiO_2, under similar layer thickness and crystal structure, the nanoporous TiO_2 generates more photo-excited electron–hole pairs and has more efficient charge separation, resulting in enhanced photoelectrochemical response. Improved photocatalytic activity is demonstrated through both the photo-degradation of methyl orange and antibacterial test of *Staphylococcus aureus*. The photocatalytic properties of nanoporous TiO_2 can be further improved if thicker TiO_2 layer is made after extended anodization. It can be expected that such nanostructured TiO_2 is promising not only in photocatalysis, but also in solar cell, water cleavage and other photoelectrochemical applications.

Acknowledgements

The work described in this paper was fully supported by a grant from the Research Grants Council of the Hong Kong Special Administrative Region, China (Project No. PolyU5166/05E) and partially supported by grants from the Hong Kong Polytechnic University (Projects Nos.: G-YE50 and A-PA6A).

References

[1] A. Mills, R.H. Davies, D. Worsley, Chem. Soc. Rev. 22 (1993) 417–425.
[2] M.R. Hoffmann, S.T. Martin, W.Y. Choi, D.W. Bahnemann, Chem. Rev. 95 (1995) 69–96.
[3] C.M. Wang, A. Heller, H. Gerischer, J. Am. Chem. Soc. 114 (1992) 5230–5234.
[4] K. Vinodgopal, S. Hotchandani, P.V. Kamat, J. Phys. Chem. 97 (1993) 9040–9044.
[5] E. Barraud, F. Bosc, D. Edwards, N. Keller, V. Keller, J. Catal. 235 (2005) 318–326.
[6] L. Armelao, D. Barreca, G. Bottaro, A. Gasparotto, C. Maccato, C. Maragno, E. Tondello, U.L. Stangar, M. Bergant, D. Mahne, Nanotechnology 18 (2007) 375709.
[7] H.F. Zhuang, C.J. Lin, Y.K. Lai, L. Sun, J. Li, Environ. Sci. Technol. 41 (2007) 4735–4740.
[8] J.M. Macak, M. Zlamal, J. Krysa, P. Schmuki, Small 3 (2007) 300–304.
[9] R. Beranek, H. Tsuchiya, T. Sugishima, J.M. Macak, L. Taveira, S. Fujimoto, H. Kisch, P. Schmuki, Appl. Phys. Lett. 87 (2005) 243114.
[10] H.E. Prakasam, K. Shankar, M. Paulose, O.K. Varghese, C.A. Grimes, J. Phys. Chem. C 111 (2007) 7235–7241.
[11] M. Paulose, K. Shankar, S. Yoriya, H.E. Prakasam, O.K. Varghese, G.K. Mor, T.A. Latempa, A. Fitzgerald, C.A. Grimes, J. Phys. Chem. B 110 (2006) 16179–16184.
[12] J.M. Macak, H. Tsuchiya, L. Taveira, S. Aldabergerova, P. Schmuki, Angew. Chem., Int. Ed. 44 (2005) 7463–7465.
[13] J.M. Macak, H. Tsuchiya, P. Schmuki, Angew. Chem., Int. Ed. 44 (2005) 2100–2102.
[14] V. Zwilling, E. Darque-Ceretti, A. Boutry-Forveille, D. David, M.Y. Perrin, M. Aucouturier, Surf. Interf. Anal. 27 (1999) 629–637.
[15] J.M. Macak, P. Schmuki, Electrochim. Acta 52 (2006) 1258–1264.
[16] J.M. Macak, S. Albu, D.H. Kim, I. Paramasivam, S. Aldabergerova, P. Schmuki, Electrochem. Solid-State Lett. 10 (2007) K28–K31.
[17] D. Gong, C.A. Grimes, O.K. Varghese, W. Hu, R.S. Singh, Z. Chen, E.C. Dickey, J. Mater. Res. 16 (2001) 3331–3334.
[18] J. Kunze, A. Seyeux, P. Schmuki, Electrochem. Solid-State Lett. 11 (2008) K11–K13.
[19] K.S. Raja, M. Misra, K. Paramguru, Electrochim. Acta 51 (2005) 154–165.
[20] Q.A. Nguyen, Y.V. Bhargava, T.M. Devine, Electrochem. Commun. 10 (2008) 471–475.
[21] N.K. Allam, K. Shankar, C.A. Grimes, J. Mater. Chem. 18 (2008) 2341–2348.
[22] G. Zhang, H. Huang, Y. Zhang, H.L.W. Chan, L. Zhou, Electrochem. Commun. 9 (2007) 2854–2858.
[23] K.S. Raja, T. Gandhi, M. Misra, Electrochem. Commun. 9 (2007) 1069–1076.
[24] C.C. Trapalis, P. Keivanidis, G. Kordas, M. Zaharescu, M. Crisan, A. Szatvanyi, M. Gartner, Thin Solid Films 433 (2003) 186–190.
[25] S.-Z. Chu, K. Wada, S. Inoue, M. Isogai, A. Yasumori, Adv. Mater. 17 (2005) 2115–2119.
[26] A.P. Li, F. Muller, A. Birner, K. Nielsch, U. Gosele, J. Appl. Phys. 84 (1998) 6023–6026.
[27] S. Berger, H. Tsuchiya, P. Schmuki, Chem. Mater. 20 (2008) 3245–3247.
[28] J.M. Macak, S. Aldabergerova, A. Ghicov, P. Schmuki, Phys. Stat. Sol. (a) 203 (2006) R67–R69.
[29] B.A. Dilmohamud, J. Seeneevassen, S.D.D.V. Rughooputh, P. Ramasami, Eur. J. Phys. 26 (2005) 1079–1084.
[30] A. Sclafani, J.M. Herrmann, J. Phys. Chem. 100 (1996) 13655–13661.
[31] B. Ohtani, Y. Ogawa, S.-I. Nishimoto, J. Phys. Chem. B 101 (1997) 3746–3752.
[32] D.W. Chen, A.K. Ray, Wat. Res. 32 (1998) 3223–3234.
[33] H. Tada, Y. Kubo, M. Akazawa, S. Ito, Langmuir 14 (1998) 2936–2939.
[34] Z.-S. Wang, C.-H. Huang, Y.-Y. Huang, Y.-J. Hou, P.-H. Xie, B.-W. Zhang, H.-M. Cheng, Chem. Mater. 13 (2001) 678–682.
[35] G.K. Mor, K. Shankar, M. Paulose, O.K. Varghese, C.A. Grimes, Nano Lett. 6 (2006) 215–218.
[36] J. Bandara, S.S. Kuruppu, U.W. Pradeep, Colloids Surf. A 276 (2006) 197–202.
[37] J.P.H. Sukamto, C.S. Mcmillan, W. Smyrl, Electrochim. Acta 38 (1993) 15–27.
[38] M. Gratzel, Nature 414 (2001) 338–344.
[39] A. Zaban, M. Greenshtein, Bisquert, J. Chem. Phys. Chem. 4 (2003) 859–864.
[40] X.Z. Li, F.B. Li, J. Appl. Electrochem. 32 (2002) 203–210.
[41] S.U.M. Khan, M. Al-Shahry, W.B. Ingler, Science 297 (2002) 2243–2245.
[42] C. Wei, W.-Y. Lin, Z. Zainal, N.E. Williams, K. Zhu, A.P. Kruzic, R.L. Smith, K. Rajeshwar, Environ. Sci. Technol. 28 (1994) 934–938.
[43] K. Sunada, T. Watanabe, K. Hashimoto, Environ. Sci. Technol. 37 (2003) 4785–4789.